THE ASTROPHYSICAL JOURNAL, 396:469–486, 1992 September 10

THE UNIVERSITY OF MICHIGAN RADIO ASTRONOMY DATA BASE. I. STRUCTURE FUNCTION ANALYSIS AND THE RELATION BETWEEN BL LACERTAE OBJECTS AND QUASI-STELLAR OBJECTS

P. A. HUGHES, H. D. ALLER, AND M. F. ALLER
Astronomy Department, University of Michigan, Dennison Building, Ann Arbor, MI 48109–1090
Received 1991 November 8; accepted 1992 March 17

ABSTRACT

We have performed a structure function analysis on a well-observed group of variable extragalactic sources, monitored in total and polarized flux in the centimeter waveband since 1965. Total flux structure functions of BL Lac objects and QSOs exhibit very similar power-law slopes, suggesting that the same processes are responsible for the variability in both types of source. In view of the recent success of the shocked-jet model for radio source variability, we argue that the current work provides circumstantial evidence for the ubiquity of such shocked flows. This analysis has provided a good estimate of characteristic time scales of variability for the two types of object: there is a very broad distribution of time scales for both BL Lac objects and QSOs, with mean time scales of 1.95 and 2.35 yr, respectively. The majority of sources ($\gtrsim 85\%$) with time scales greater than 10 yr are QSOs. A structure function analysis applied to the Stokes parameters in a frame of reference related to the VLBI jet structure suggests that variations of the polarized flux occur in an orientation related to the underlying jet direction. This is further circumstantial evidence for the domination of the source polarization by a shock phenomenon, as this behavior is what one would expect from the axial compression of a turbulent magnetic field. We interpret our derived time scales for Q and U variations and the relative amplitude of these variations, in terms of emission from shocked jets with a well-defined magnetic field direction, contaminated by a significant but randomly polarized core emission for BL Lacs, and in similar terms, but with a magnetic field less strongly correlated with the jet direction, and a weakly polarized core, for QSOs. Periodogram analyses show little or no evidence of harmonic behavior.

Subject headings: BL Lacertae objects: general — galaxies: jets — polarization — quasars: general — radio continuum: galaxies

1. INTRODUCTION

The University of Michigan 26 m paraboloid has been used to monitor variable, compact radio sources in both total and linearly polarized flux for over 25 years. At 4.8 GHz observations were started on a regular basis in 1978, at 8.0 GHz in 1965, and at 14.5 GHz in 1974. Over the years new sources have been added to the observing schedule, and so time coverage varies from source to source, and frequency to frequency. Nevertheless, the data base provides high-quality, high time resolution (better than 1 month) multifrequency data spanning more than one decade, for many sources. Details of the observing program and monthly averaged data for the best-observed sources may be found in Aller et al. (1985); data for the period $\gtrsim 1985.0$ are to be published shortly.

Although some source activity, particularly at low frequency, may be of extrinsic origin (e.g., Padrielli et al. 1987), an attractive hypothesis is that much of the activity observed in the centimeter-wavelength band can be explained as due to the propagation of shocks. We have had considerable success in modeling a number of the outbursts that are distinct in total flux, polarized flux, or both. These models involve shocks in collimated, relativistic flows. Their primary features are (1) that the rise and fall of the total flux are associated with the passage of the shocked region through the $\tau = 1$ surface of the flow, and its subsequent energy loss due to adiabatic expansion; and (2) that the increase in percentage polarization is a consequence of the compression, by the shock, of a tangled magnetic field. Maps derived from the models—constrained only by the single dish data—agree with coeval VLBI maps, supporting the idea that many or all outbursts seen in the monitoring data correspond to the propagation of individual components on VLBI maps. Details of this modeling are described in Hughes, Aller, & Aller (1989a, b; 1991). However, such modeling has been restricted to a few sources with isolated, well-defined events. To test the hypothesis that the same mechanism can account for the activity in all sources we have performed a statistical analysis of a large sample of particularly well-observed sources from the monitoring program. As described here, such an analysis suggests that most activity has a common physical origin; this in conjunction with the success of the shock model, provides evidence for the ubiquity of shocks in parsec scale flows.

Structure function analysis provides a method of quantifying time variability without the problems of windowing, aliasing, etc., that are encountered in the traditional Fourier analysis technique. It can potentially provide information on the nature of the process that causes variation and has been used by a number of authors to study intrinsic variations of AGNs (e.g., Bregman et al. 1988) and radio source scintillation (e.g., Simonetti, Cordes, & Heeschen 1985). We have found this method of analysis to be a fruitful way of characterizing the variability exhibited by sources in the UMRAO program, and in this paper we present the results of performing a first-order structure function analysis on a subset of the UMRAO sources. In § 2 we describe our analysis of the total flux variations; in § 3 we describe how a similar analysis was applied to the polarized

flux; and in § 4 we discuss our results, briefly describe a periodogram search for harmonic behavior in the variations, and give our conclusions.

2. STRUCTURE FUNCTION ANALYSIS OF THE TOTAL FLUX

2.1. *Properties of Structure Functions*

The general definition of structure functions and some of their properties are given by Simonetti et al. (1985). Here we use only the first-order structure function, which is defined as $D^1(\tau) = \langle [S(t) - S(t+\tau)]^2 \rangle$, $S(t)$ being the signal (flux) at time t, and τ being the "lag." It is commonly characterized in terms of its slope: $b = d \log D^1 / d \log \tau$. For a stationary random process the structure function is related simply to the variance of the process (σ^2) and its autocorrelation function [$\rho(\tau)$] by $D^1(\tau) = 2\sigma^2[1 - \rho(\tau)]$. Figure 1 shows schematically the structure function of a "typical" measured process. For lags longer than the longest correlation time scale, there is a plateau with an amplitude equal to twice the variance of the fluctuation. For short time lags, the plateau is just twice the variance of the measurement noise, because this (assumed Gaussian) has a zero correlation time scale. These regions are linked by a curve whose slope depends on the nature of the intrinsic variation of the source (e.g., shot noise, flicker noise, etc.).

The structure function, autocorrelation function, and power spectrum [$P(f)$] are related measures of the distribution of power with time scale. Any of these measures for a real process will be a nonsimple function of time lag (or frequency); however, certain simple forms make useful reference: If $P(f) \propto f^{-1}$, then $D^1(\tau) \propto \tau^0$. This is often called *flicker* noise, and there is equal power in equal logarithmic frequency intervals. Such noise may be generated by the sum of the slowly decaying responses to white-noise impulses, although the particular spectral slope requires the "right" distribution of response time scales (Dutta & Horn 1981). Flicker noise exhibits both short time-scale fluctuations, and long time-scale trends, and neither the local value nor the mean are well defined. If $P(f) \propto f^{-2}$, then $D^1(\tau) \propto \tau^1$. This is called *short* or *random walk* noise, and there is much more power at low than at high frequency. Such noise also may be generated by filtering white noise, and it is the high-frequency limiting form of the resultant power spectrum, regardless of the distribution of response times (assuming that the signal's spectrum can be approximated by the inverse quadratic form associated with a first-order autoregressive process); however, it is most easily understood as due to a random walk, for example, the sum of random numbers generated on the interval [−1, 1]. The value at a particular time is well defined, but by the nature of the random walk there is no well-defined mean as the process continues for arbitrary times. Press (1978) gives a comprehensive discussion of these types of noise.

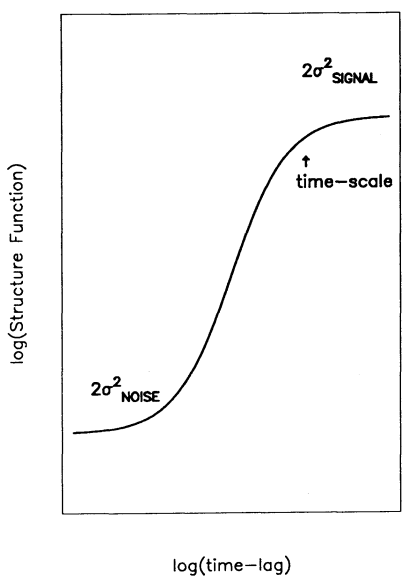

FIG. 1.—Schematic showing the "ideal" structure function for a time series plus measurement noise.

The potentially multislope form of the power spectrum leads to an ambiguity in the interpretation of the structure function. A short time-lag plateau is reasonably interpreted as due to measurement noise and is of no intrinsic interest. A τ^1 form at somewhat longer time-lags corresponds to "random walk" or "shot" noise and can reasonably be interpreted as indicating that we are looking at a "shot process": slowly decaying responses to white-noise impulses. In the current study this would lead to the conclusion that the shocks are caused by random disturbances, rather than by some regular or cyclic mechanism. At longer time lags we begin to see a flattening of the structure function. However, this may be interpreted in two ways: such a form will arise if the f^{-2} part of the power spectrum matches without discontinuity with a f^0 segment corresponding to time lags great enough that the signal is uncorrelated. The time lag of the turnover in the structure function then measures *the minimum time scale of uncorrelated behavior*. It is quite possible, however, that there is a domain of f^{-1} noise for $f_1 < f < f_2$, and we would expect from dimensional arguments (see above) that such a domain also would lead to a flattening of D^1. This may be confirmed by a simple illustrative example—for instance, taking a cosine transform of a three-slope power spectrum; it will be seen that the structure function swings from the τ^1 asymptote to the τ^0 asymptote between $\tau \sim 1/2\pi f_2$ and $\tau \sim 1/f_2$. (The apparent paradox that two distinct slopes in the power spectrum both contribute to the flat portion of the structure function is resolved by remembering that the f^0 segment contributes only a delta-function at $\tau = 0$ in the temporal domain.) If, as seems plausible, the flicker noise part of the spectrum arises because of the distribution of response times to the impulses over some domain $f_1 < f < f_2 (\tau_2 < \tau < \tau_1)$, then the turnover in the structure function at $\tau \sim \tau_2$ measures *the minimum time scale in the distribution of response times*. We cannot easily distinguish these two cases (see below), but either way, the time scale derived from the plateauing of the structure function is a robust, physically meaningful characteristic time scale for each source, which can be compared from source to source, and for different classes of sources.

Ideally such an analysis performed for a set of sources will yield a set of curves similar to that in Figure 1, from which we can determine the characteristic time scales (from the time lag at which the curves plateau) and an indication of the nature of the process of variation (from the slope of the "power-law" portions of the curves). To facilitate the estimate of when the long time-lag plateau occurs, we have normalized all structure functions with σ^2: curves should asymptote to log (2.0) ~ 0.3. In the majority of cases we find that a little smoothing of the structure function produces something very close to the ideal form from which we can unambiguously determine a time scale

and a slope. However, in a few cases the structure function deviates quite significantly from the ideal.

Types of behavior exhibited are the following: (1) Sources which display no plateau at long time lag: here we make the interpretation that the characteristic time scale is longer than is detectable by the current time base of the data, and the longest time lag available sets a lower limit on the characteristic time scale. (2) Sources with a third plateau at intermediate time lag: here we assume that we are seeing the signature of two distinct processes; in some cases the shorter time scale one may be due to interstellar scintillation (e.g., Spangler et al. 1989), and we use the longer time lag plateau to derive values for the intrinsic process. (3) Sources with a very irregular structure function: in general, variations dominated by one or a few large outbursts, or variations that are more or less periodic, will have such behavior reflected in the structure function; in most cases we can identify large excursions in the structure function with such behavior and derive a slope (although not always a time scale) by fitting a mean slope through the rising part of the structure function.

A complicating factor in interpreting the computed structure functions is that at long time lag the structure function will often undergo a rapid rise, fall, or oscillation: this is an erratic behavior associated with the chance value of points at the ends of the data train—we do not consider the structure function to be well defined there and use only the curve at shorter time lag to derive values. In these cases we often get only a limit on the characteristic time scale. Finally we note that a linear trend will contribute to the structure function as τ^2. The light curves show few cases where it would appear appropriate to remove such a trend (there being long-term variations, but not such as extend coherently over the entire time base); furthermore, if such trends were important, they would show up as steep portions to the structure functions—which in general we do not see (but note the discussion of steep structure functions in § 2.2.1).

In the vast majority of sources the well-defined non-zero slope extends so close to the long time lag limit (set by the length of the data series) that determining whether there is a domain of flicker noise is essentially impossible. In principle, we could look for the signature of flicker noise in the power spectrum. This, however, is not viable: we are too close to the frequency corresponding to the overall window of observation to get a well-defined spectral form—and suffer the usual additional problems of "messy windows" and aliasing in the frequency domain.

2.2. *Results for the Total Flux Variability*

The number of daily observations in the UMRAO data base has approximately doubled since the major data summary in 1985 (Aller et al. 1985), a reflection of the efficiency of automated observing. However, in order to ensure not only a number of observations sufficient to generate well-defined structure functions, but also observations spanning a time period sufficient to probe both short and long time scales, we have selected for this analysis only sources with more than 300 observations *before* ~1985. We have used a cutoff date for the analysis of 1991.0. The starting date of observations and number of observations at each observing frequency are given for the selected 51 sources in Table 1. General parameters for these sources are collected together in Table 2 and will be discussed below.

We have computed structure functions at each of the three observing frequencies for time lags ranging from ~2 weeks to 10 yr, and a sample of these are shown in Figures 2*a*–2*h*. The short-dashed horizontal line is the expected 2 σ^2 asymptote discussed above. The normalization tends to bring together the structure function curves at each of the observing frequencies. The solid line is a fit to the structure function between time lags that appear to delineate the anticipated "power-law" portion of the function. (This is a mean of all three frequencies, unless one or more frequency has been excluded as "pathological"—see the notes to Table 3.) The long-dashed horizontal line is an estimate of the contribution to the structure functions from the Gaussian noise in the data: we have used a mean of error estimates at the three frequencies, weighted by the number of observations at each. We could have subtracted this estimated contribution due to measurement noise from the structure functions, before exploring the log D–log τ plane. However, the estimate of the Gaussian noise contribution is just that—an estimate. For data gathered over so long a time span, the magnitude of the errors changes on both short time scales due to particularities of observing conditions, and on longer time scales because of improvements in and degradation of receivers, for example. We have explored the distribution of errors by source and frequency and conclude that although the above estimate is reasonable, it is too imprecise to be of use if subtraction of this term is important—and there is no compelling reason to subtract it otherwise. As we note later (see § 3), it is not important, and so we choose to indicate the possible contribution, but present and work with the "raw" structure functions.

Figures 2*a*–2*b* show structure functions that exhibit a well-defined turnover to the expected asymptote, while Figures 2*c*–2*d* show structure functions that do not display a plateau. Figure 2*d* shows the erratic behavior that is often associated with long time lag because of the finite range of the time series. We find that $\gtrsim$65% of the structure functions are as well defined as those shown in Figures 2*a*–2*d* (albeit that the plateau is not always very flat—oscillations associated with long-time-scale, large-amplitude fluctuations are sometimes evident); $\gtrsim$25% of the structure functions exhibit some "abnormality" which makes it more difficult to estimate their slope. Examples of these are shown in Figures 2*e*–2*f*. The vertical separation with frequency for 3C 120 arises because the time series at 8.0 GHz covers a much greater time span, and it includes major outbursts in the early 1970s, before most of the 14.5 GHz data, and essentially all the 4.8 GHz data, were obtained. The absolute value of the variance is highest at 8.0 GHz, and since that is used in normalization, it "suppresses" the structure function at this frequency. 0754+100 (Fig. 2*f*) is typical of a few sources that appear to display an intermediate time lag plateau. The time scale (3–4 months) is of the right order to be associated with refractive interstellar scintillation (RISS), and although this source has a Galactic latitude of ~19°, which might seem rather high for scintillation effects to occur, we note that the dependence of RISS on Galactic latitude is weak (Spangler et al. 1989). The notes accompanying Table 3 give the Galactic latitude of the four sources that display evidence of a "second" process—possibly RISS; all have $b \lesssim 30°$ and three have $b \lesssim 20°$. These time scales and Galactic latitudes are consistent with a RISS origin for the intermediate plateau, but this is rather weak evidence. However, even if the plateau arises from an intrinsic process, the few sources with this characteristic behavior will not significantly influence our overall conclusions. Figures 2*g*–2*h* show examples of sources with "abnormally" flat or steep structure functions.

In all the cases discussed above we used that frequency (or frequencies) with the best-defined power-law segment to derive slope and time-scale values. The values are listed in Table 3, and the notes associated with that table comment on particular features of the structure functions that were relevant to the derivation of these numbers. Some sources (e.g., 3C 345) do not exhibit an unambiguous plateau, but rather a peak or small oscillation in the structure function at long time lag. A reasonable interpretation of this is a plateau slightly masked by the contribution of long-term trends or a few large outbursts. However, in such cases we have conservatively taken the turnover from the power-law portion of the structure function as a *lower limit* to the time scale. Visual inspection of the whole set of structure functions suggests that BL Lac objects exhibit plateaus and have shorter characteristic time scales than do QSOs—here the structure functions often appear to rise until longer time lag effects begin to play a role. However, as we discuss below, we find such a larger range of time scales within each group that our quantitative analysis provides only weak evidence for a difference in BL Lac and QSO time scales.

2.2.1. *Time Scales and Slopes*

The distributions of time scales and slopes are shown in Figures 3*a*–3*c*, and the parameter values used in the following discussion are those in Tables 2 and 3. Figure 3*a* shows the distribution of time scales for all sources, BL Lac objects and

TABLE 1

SOURCES: SUMMARY OF OBSERVATIONS

SOURCE	POSITION NAME	4.8 GHz		8.0 GHz		14.5 GHz	
		Start	Number of Observations	Start	Number of Observations	Start	Number of Observations
III Zw 2	0007+106	80.0	88	76.1	326	78.3	189
0048−097	0048−097	80.7	133	69.7	292	74.7	247
DA 55	0133+476	79.4	337	71.3	589	74.5	421
0235+164	0235+164	77.8	368	74.6	792	75.7	549
OE 400	0300+470	77.8	224	75.9	691	78.3	397
OE 110	0306+102	80.1	66	78.2	384	79.7	191
3C 84	0316+413	77.8	320	65.5	1225	74.1	498
NRAO 140	0333+321	80.8	153	78.4	406	80.0	241
CTA 26	0336−019	79.6	76	66.5	395	74.7	283
NRAO 150	0355+508	77.8	158	66.6	776	74.4	425
3C 111	0415+379	77.8	102	75.9	432	75.9	200
0420−014	0420−014	78.5	369	77.4	767	77.6	425
OF 038	0422+004	80.1	104	78.8	400	79.7	263
3C 120	0430+052	78.3	382	66.6	1154	74.4	595
0528+134	0528+134	80.8	66	76.3	281	80.7	99
0607−157	0607−157	78.0	348	74.8	692	77.6	480
0727−115	0727−115	77.8	399	71.3	830	74.5	492
0735+178	0735+178	79.3	277	77.2	603	77.6	374
OI 90.4	0754+100	80.1	88	78.1	245	78.9	222
0814+425	0814+425	77.8	109	77.4	452	77.6	198
OJ 287	0851+202	78.3	398	71.1	933	74.3	625
4C 39.25	0923+392	77.8	286	67.1	972	74.3	485
1055+018	1055+018	78.2	119	67.1	393	74.3	227
1127−145	1127−145	78.0	291	67.3	860	74.4	415
1156+295	1156+295	81.4	191	77.4	496	80.4	322
3C 273	1226+023	78.3	275	65.5	1041	74.3	495
3C 279	1253−055	78.0	362	65.6	1023	74.3	506
1308+326	1308+326	78.7	329	76.3	817	76.4	531
1335−127	1335−127	80.0	248	74.7	570	74.7	336
1413+135	1413+135	80.7	227	78.1	572	80.4	355
1418+546	1418+546	80.1	276	78.6	585	79.3	433
1510−089	1510−089	78.3	332	74.7	767	74.6	436
4C 14.60	1538+149	80.6	101	77.4	353	79.7	223
3C 345	1641+399	78.0	461	65.6	1228	74.3	590
Mrk 501	1652+398	79.6	87	78.0	329	79.3	154
NRAO 530	1730−130	77.8	218	67.3	668	74.3	380
OT 081	1749+096	80.0	375	78.3	656	78.9	447
1749+701	1749+701	80.6	119	80.1	289	80.2	170
3C 371	1807+698	80.1	130	79.4	413	79.7	200
OV−236	1921−293	77.8	312	74.7	689	74.6	495
OV−198	1958−179	81.2	30	78.4	295	79.3	112
2005+403	2005+403	77.8	170	75.2	523	75.2	402
3C 418	2037+511	77.8	66	66.5	399	74.4	110
OX 036	2121+053	78.0	195	76.4	649	77.6	319
2131−021	2131−021	80.6	83	74.9	235	80.3	218
2134+004	2134+004	77.8	157	67.6	589	74.4	288
2145+067	2145+067	80.6	196	67.6	624	74.5	385
BL Lac	2200+420	77.8	488	68.3	1151	74.4	748
3C 446	2223−052	78.0	287	67.1	604	74.6	347
CTA 102	2230+114	81.4	183	74.6	618	79.8	420
3C 454.3	2251+158	77.8	368	66.5	1076	74.1	560

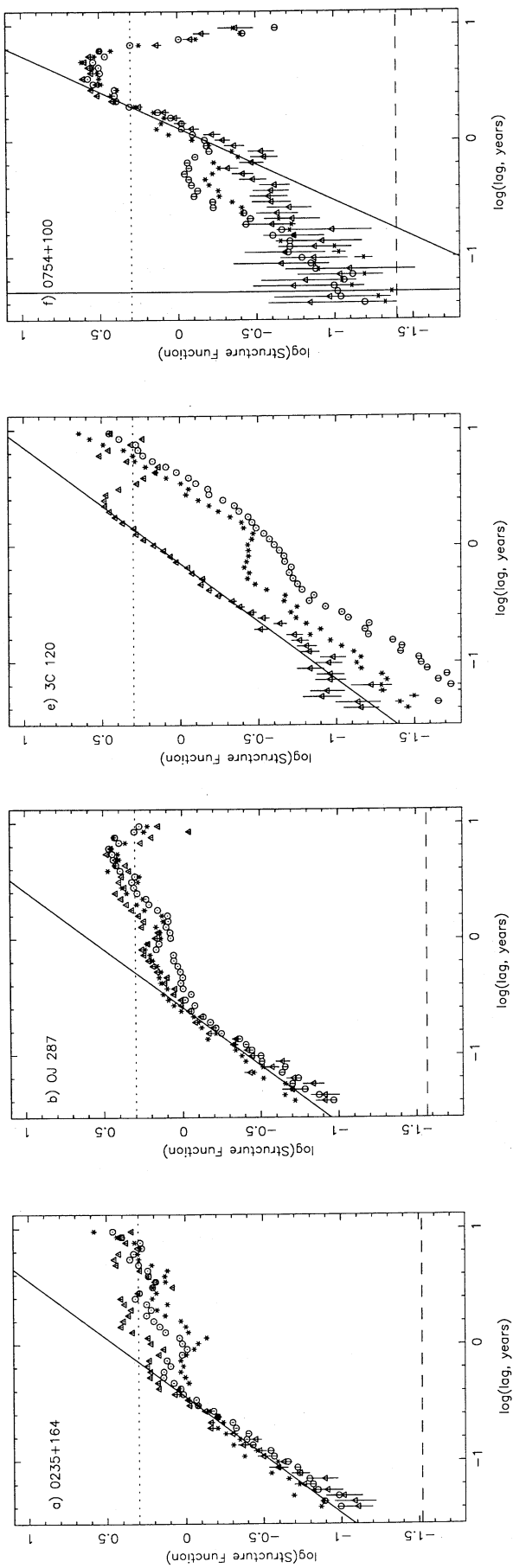

FIG. 2.—Examples of the structure functions for total flux variations. Triangles denote 4.8 GHz observations, circles are 8 GHz observations, and crosses are 14.5 GHz observations. The short-dashed horizontal line shows the anticipated long time lag plateau (having normalized the function with the variance, σ^2, at each frequency), and the solid line is our estimate of the slope in the power-law portion of the curve. The long-dashed horizontal line indicates the anticipated contribution from measurement error.

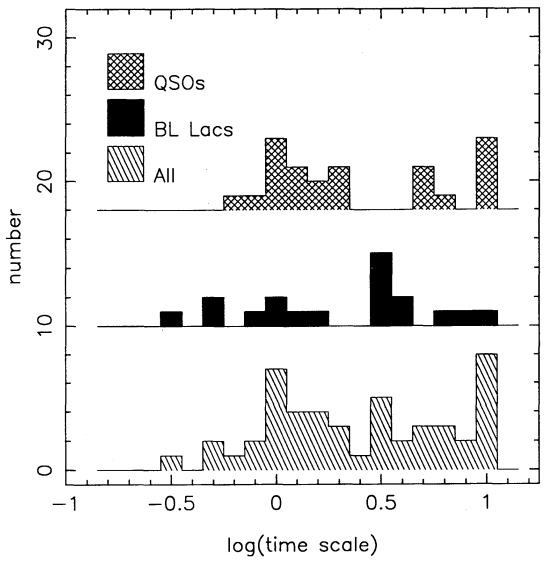

FIG. 3a

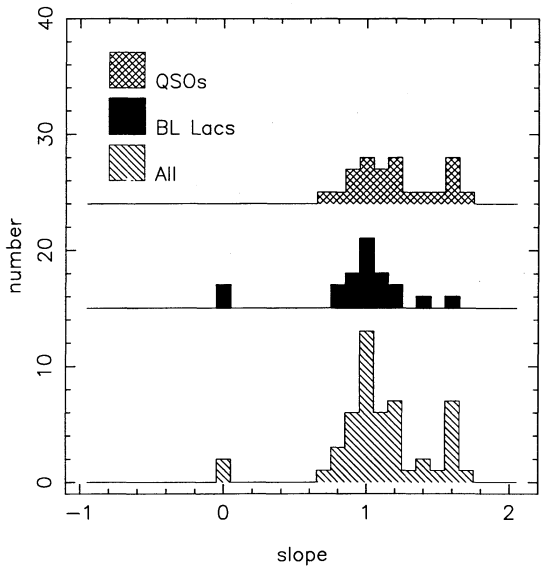

FIG. 3b

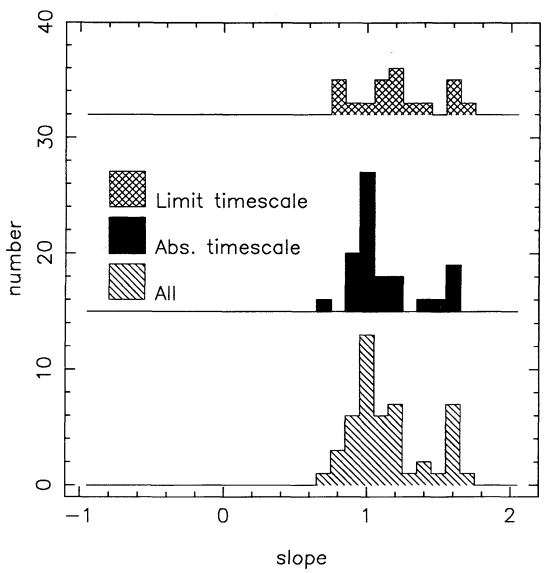

FIG. 3c

FIG. 3.—(*a*) Distribution of characteristic time scales estimated from the total flux structure functions for all sources in the sample, BL Lac objects, and QSOs. (*b*) Distribution of slopes estimated from the total flux structure functions for all sources, BL Lac objects and QSOs. (*c*) Distribution of slopes as shown in Fig. 3*b*, subdivided by whether we have been able to estimate an absolute characteristic time scale, or only a lower limit.

QSOs. Lower limits have been plotted as actual values. It appears that there is no significant differences between the distribution of BL Lac objects and QSOs. As the histogram might be misleading through its failure to show lower limits, we have applied statistical tests from the "Two-Sample Test" package (ASURV: Feigelson & Nelson 1985; Isobe, Feigelson, & Nelson 1986) which enable us to incorporate information about the lower limit values. The results are shown in Table 4. All four tests available to us indicate that the results are consistent (at better than the 80% level) with the BL Lac and QSO time distributions being derived from the same parent population. (This statistic may not be very sigificant—but the essential point is that there is no strong evidence for two distinct populations.)

The distribution of slopes is shown in Figure 3*b*. It is immediately evident that for most sources $b_S \sim 1$. The two sources with $b_S \sim 0$ are Mrk 501 and 3C 371, for which both the asymptotic value of the structure functions and the light curves appear to indicate a low level of uncorrelated fluctuation: we seem to be seeing no more than white noise. All sources, whether BL Lac objects or QSOs, with $b_S \gtrsim 1.5$ have light curves that are dominated by one or a few prominent outbursts, and in these sources the portion of the structure function that we select as being the "power-law" part has its form determined largely by a few large-amplitude variations exhibited by the light curves: as noted in § 2.1, linear trends will steepen the structure function. It is possible that over a much greater timespan, these sources would exhibit variations that better approximate stationary noise. The majority of sources *do* have light curves that appear reasonably to approximate a random process and have b_S very near to unity. This can be seen from Table 5, where we list the slopes for all sources, and subsets by source type and by location with respect to the peak at $b_S \sim 1$. Considering only those sources within this dominant peak, the value of $\langle b_S \rangle$ for BL Lac objects and QSOs is the same to within the dispersion. The same set of statistical tests applied to the time scales (see Table 4) shows that for the sample as a whole, there is a low probability that BL Lac objects and QSOs derive from the same parent population. This is because the two flat structure function sources are BL lac objects, while the sources with $b_S \gtrsim 1.5$ are preferentially QSOs. Considering only those sources in the central peak about $b_S \sim 1$ shows that there is no significant difference between the two classes (Table 4, last column). Figure 3*c* shows that there is no correlation between slope and whether or not we have only a lower limit to the time scale.

We conclude that on the basis of time scales and slopes, there is no significant difference between BL Lac objects and QSOs. More than 50% of those sources with $b_S \gtrsim 1.5$ have a well-determined time scale (as opposed to a lower limit); if these estimates are spurious (because we are not looking at the

TABLE 2

SOURCES: GENERAL PARAMETERS

SOURCE (1)	TYPE (2)	z (3)	S_{365}[a] Value (4)	S_{365}[a] Source (5)	$\mathscr{V}$ (6)	V(14.5) (7)	V(4.8) (8)	ROTATION MEASURE[b] Value (9)	ROTATION MEASURE[b] Source (10)	P.A.[c] Value (11)	P.A.[c] Source (12)
III Zw 2	Q	0.089	...	...	...	0.770	0.795	...	...	180.0	j85
0048−097	BL	0.475*	1.28	k	0.900	0.543	0.357	−5.0	sn	...	...
DA 55	Q	0.860	2.07	k	0.300	0.390	0.363	109.0	ru	125.0	r85, m80
0235+164	BL	0.940	1.90	k	0.900	0.828	0.670	57.0	ru	20.0	i87, r85
OE 400	BL	0.475*	...	...	...	0.461	0.344	11.0	rj	90.0	g90
OE 110	BL	0.475*	...	...	0.290	0.516	0.282	...	...	−135.0	g90
3C 84	G	0.017	38.50	k	0.005	0.325	0.215	76.0	ru	12.0	i87
NRAO 140	Q	1.258	7.07	p	0.700	0.491	0.276	56.0	ru	132.0	i87, r85, m87, o88
CTA 26	Q	0.852	1.90	k	0.520	0.303	0.231	17.0	sn	60.0	w91
NRAO 150	EF	...	...	...	0.069	0.731	0.522	−17.0	ru	70.0	r85, j85
3C 111	NG	0.049	33.30	e	0.020	0.514	0.057	−21.0	ru	63.0	r85
0420−014	Q	0.915	1.85	k	...	0.339	0.283	−13.0	rj	90.0	w91
OF 038	BL	0.475*	...	...	0.600	0.589	0.367	...	...	40.0	p86
3C 120	G	0.033	5.11	k	0.070	0.763	0.341	−1.0	ru	−103.0	r85, w88
0528+134	RSO	...	...	...	...	0.183	0.132	...	...	...	...
0607−157	Q	0.324	3.39	k	0.270	0.922	0.791	55.0	ru	38.0	r85, r84, p86
0727−115	...	...	...	...	...	0.605	0.520	...	...	...	...
0735+178	BL	0.424	2.35	k	0.300	0.614	0.467	9.0	ru	65.0	i87, w88, r85, g89, o88
OI 90.4	BL	0.475*	...	...	...	0.627	0.530	29.0	rj	30.0	g90
0814+425	BL	0.475*	2.88	k	0.600	0.489	0.608	19.0	ru	−31.0	p88
OJ 287	BL	0.306	0.86	k	...	0.709	0.578	31.0	ru	−108.0	w88, g89
4C 39.25	Q	0.699	4.37	k	0.250	0.500	0.202	15.0	ru	−75.0	i87, b87, ma90, z90
1055+018	Q	0.888	4.17	k	0.490	0.330	0.134	−37.0	ru	−55.0	o88
1127−145	Q	1.187	5.63	k	...	0.268	0.126	34.0	ru	62.0	w91
1156+295	Q	0.729	2.17	c	0.330	0.593	0.344	−36.0	sn	22.0	m89
3C 273	Q	0.158	62.50	k	...	0.400	0.137	2.0	ru	−117.0	r85, b87
3C 279	Q	0.538	15.30	k	0.310	0.199	0.161	27.0	ru	−133.0	r85, b87
1308+326	BL	0.996	1.24	k	...	0.718	0.558	−4.0	ru	−30.0	r85
1335+127	BL	0.541	2.22	g	0.550	0.548	0.517	...	...	...	...
1413+135	BL	0.260	...	...	0.090	0.596	0.364	...	...	...	...
1418+546	BL	0.475*	1.87	k	0.600	0.555	0.472	17.0	rj	...	...
1510−089	Q	0.361	3.76	k	0.730	0.654	0.629	−13.0	ru	173.0	r85, o88
4C 14.60	BL	0.475*	3.17	k	0.300	0.499	0.307	17.0	ru	−44.0	r85, g90
3C 345	Q	0.595	10.30	k	0.280	0.555	0.350	26.0	ru	−135.0	h88
Mrk 501	BL	0.034	1.79	k	...	0.133	0.178	42.0	ru	128.0	p88
NRAO 530	Q	0.902	11.60	p	...	0.460	0.221	−63.0	ru	−7.0	r85, r84
OT 081	BL	0.322	0.95	k	0.690	0.704	0.568	105.0	ru	67.0	w91
1749+701	BL	0.770	3.90	k	0.310	0.472	0.616	16.0	ru	−60.0	i87, r85, o88
3C 371	BL	0.050	3.23	k	0.330	0.228	0.122	5.0	ru	−97.0	i87, r85, o88
OV−236	Q	0.352	5.30	o	...	0.565	0.306	...	...	...	...
OV−198	Q	0.650	0.76	k	0.710	0.764	0.537	...	...	...	...
2005+403	Q	1.736	...	...	0.033	0.442	0.282	...	...	...	...
3C 418	Q	1.686	7.30	e	0.110	0.326	...	−29.0	ru	15.0	r85
OX 036	Q	1.878	...	...	0.650	0.721	0.753	...	...	...	...
2131−021	BL	0.557	1.97	k	0.590	0.580	0.478	10.0	sn	...	...
2134+004	Q	1.936	1.74	k	0.120	0.257	0.105	38.0	ru	62.0	r85
2145+067	Q	0.990	4.14	k	0.390	0.462	0.297	...	...	−138.0	w91
BL Lac	BL	0.070	6.70	k	0.170	0.818	0.722	−205.0	ru	−170.0	r85, mu90, w88
3C 446	Q	1.404	14.40	k	0.150	0.458	0.288	−22.0	ru	100.0	i87, c, r85
CTA 102	Q	1.037	8.00	k	...	0.374	0.127	−50.0	ru	155.0	i87, c, w
3C 454.3	Q	0.859	7.50	k	0.320	0.557	0.385	−44.0	ru	−65.0	r85, r84

NOTES.—Cols. (2) and (3): source type (BL: BL Lac object; Q: QSO; G: galaxy; NG: N-galaxy; RSO: red stellar object; EF: empty field; no entry: unknown) and redshift. These values are maintained with the UMRAO data base and updated from the literature as appropriate (e.g., Aller et al. 1985). An asterisk marks BL Lac redshifts assigned from the mean of those known; Cols. (4)–(5): 365 MHz flux in Jy; Col. (6): visibility from Preston et al. 1985; Cols. (7)–(8): variability index at 14.5 and 4.8 GHz, computed from the UMRAO data as described in the text; Cols. (9)–(10): rotation measure in rad m^{-2} used to derotate the $Q-U$ values; Cols. (11)–(12): estimate of the position angle of the VLBI structure. (For III Zw 2 we have used the value quoted for the arcsecond structure.)

[a] C: Colla et al. 1970; e: Edge et al. 1959; g: Gregorini et al. 1984; k: Kühr et al. 1981; o: Kraus & Andrew 1971; p: Pauliny-Toth, Wade, & Heeschen 1966.

[b] RJ: Rudnick & Jones 1983; ru: Rusk 1988; sn: Simard-Normandin, Kronberg, & Button 1981.

[c] We cite those sources that are more or less in agreement on the value of the VLBI position angle in each case: b87: Brown 1987; c: Cohen (unpublished); g89: Gabuzda et al. 1989; g90: Gabuzda, in preparation (quoted by Mutel 1990); h88: Hardee 1988; i87: Impey 1987; j85: Jones et al. 1985; m80: Marscher & Shaffer 1980; m87: Marscher 1987; m89: McHardy 1989; ma90: Marcaide et al. 1990; mu90: Mutel et al. 1990; o88: O'Dea et al. 1988; p86: Padrielli et al. 1986; p88: Pearson & Readhead 1988; r84: Romney et al. 1984; r85: Rusk & Seaquist 1985; w88: Wardle & Roberts 1988; w: Wehrle (unpublished); w91: Wehrle et al. 1991; z90: Zhang et al. 1990.

TABLE 3

STRUCTURE FUNCTION PARAMETERS

Source	b_S	log (τ_S)	b_Q	log (τ_Q)	b_U	log (τ_U)
III Zw 2	1.00	−0.05	0.14	−0.18	0.28	−0.85
0048−097	1.00	−0.50	0.24	−0.50	0.37	−0.20
DA 55	0.90	0.20	0.34	−0.30	0.41	−0.30
0235+164	1.00	−0.30	0.39	−0.31	0.32	−0.58
OE 400	0.90	0.10	0.64	>1.00	0.47	−0.15
OE 110	0.90	>1.00	0.11	...	0.08	...
3C 84	1.60	>0.90	0.11	...	0.12	...
NRAO 140	1.60	>1.00	0.01	...	0.00	...
CTA 26	0.85	0.30	0.14	0.00	0.11	0.00
NRAO 150	1.55	>1.00	0.78	>1.00	0.74	>1.00
3C 111	1.00	0.40	0.00	...	0.01	...
0420−014	1.20	0.20	0.57	0.03	0.57	0.09
OF 038	0.90	−0.10	0.17	−0.70	0.34	−0.30
3C 120	1.00	0.15	0.33	>1.00	0.23	>1.00
0528+134	1.20	>1.00	0.31	−0.28	0.40	−0.21
0607−157	1.30	>0.70	0.32	−0.27	0.06	...
0727−115	1.00	>0.80	0.41	−0.22	0.56	−0.28
0735+178	1.20	0.45	0.21	−0.10	0.53	−0.18
OI 90.4	1.60	0.50	0.43	−0.40	0.60	−0.52
0814+425	1.20	>0.90	0.26	−0.25	0.40	−0.69
OJ 287	1.00	−0.30	0.61	0.24	0.57	−0.26
4C 39.25	1.50	0.80	0.64	0.70	0.45	0.50
1055+018	1.00	−0.20	0.47	0.01	0.47	−0.25
1127−145	0.90	0.10	0.51	0.20	0.15	...
1156+295	1.00	−0.10	0.07	...	0.75	>1.00
3C 273	1.15	>0.65	0.84	>1.00	0.67	>1.00
3C 279	1.10	0.25	0.82	0.27	0.67	0.33
1308+326	1.05	0.45	0.41	−0.10	0.82	>1.00
1335−127	1.10	>0.50	0.57	>0.80	0.42	0.09
1413+135	0.80	>0.60	0.10	...	0.07	...
1418+546	1.00	−0.05	0.21	0.04	0.25	−0.17
1510−089	0.95	0.00	0.50	−0.20	0.42	−0.21
4C 14.60	0.95	0.20	0.50	0.09	0.40	0.13
3C 345	1.40	>0.70	0.92	0.20	0.61	0.23
Mrk 501	0.00	...	−0.08	...	−0.04	...
NRAO 530	0.80	>1.00	0.38	>1.00	0.36	>1.00
OT 081	0.80	>0.55	0.45	0.15	0.45	−0.16
1749+701	1.10	>0.80	0.39	0.10	0.18	−0.10
3C 371	0.00	...	0.13	...	0.20	...
OV−236	1.10	0.05	0.88	−0.35	0.74	−0.20
OV−198	1.15	0.00	0.20	...	0.22	...
2005+403	1.20	>1.00	0.50	0.40	0.16	0.20
3C 418	...	...	...	...	...	...
OX 036	1.55	0.00	0.37	0.05	0.28	0.00
2131−021	1.35	0.50	0.33	>1.00	0.27	−0.40
2134+004	1.10	>1.00	0.80	>1.00	0.98	>1.00
2145+067	1.65	>1.00	0.11	−0.20	0.09	−0.20
BL Lac	1.00	−0.05	0.80	−0.16	0.38	0.05
3C 446	1.60	0.10	0.24	0.21	0.45	−0.08
CTA 102	0.70	−0.05	0.06	...	0.90	>1.00
3C 454.3	1.55	0.25	0.46	>0.80	0.56	>0.80

NOTES ON INDIVIDUAL OBJECTS.—III Zw 2: Plateau poorly defined because of large-amplitude fluctuations on long time scales. 0048−097: Noisy 4.8 GHz curve ignored; 8.0 GHz variance inflated by long time-scale trends. DA 55: 8.0 GHz variance slightly inflated by long time-scale trends. OE 400: Value from 14.5 GHz data: 8.0 and 4.8 GHz slope is flatter but poorly defined. OE 110: Noisy and poorly defined. 3C 111: Value from 8.0 GHz data: 14.5 and 4.8 GHz curves very poorly defined. 0420−014: 14.5 GHz slope is flatter and less well defined. 3C 120: Value from 4.8 GHz data. 14.5 and 8.0 GHz curves show inflection between regions of similar slope, and no plateau. 0528+134: Noisy and poorly defined. 0735+178: Plateau poorly defined at 14.5 and 4.8 GHz. OI 90.4: Strong evidence of plateau, albeit above the anticipated 2 σ^2 level. Strong evidence of intermediate time lag plateau, perhaps associated with extrinsic variability ($b \sim 19°$). OJ 287: Gradual turnover makes time-scale estimate uncertain. 1055+018: Poorly defined, and gradual turnover makes time-scale estimate uncertain. 1127−145: Poorly defined at 8.0 GHz; no well-defined form at 14.5 and 4.8 GHz. 1418+546: Poorly defined curve at 14.5 GHz. 4C 14.60: Plateau is rather poorly defined. Mrk 501: Flat—consistent with an uncorrelated stationary process. NRAO 530: Values from 8.0 GHz data. A suggestion of intermediate time-lag plateau at 14.5 and 4.8 GHz, perhaps associated with extrinsic variability ($b \sim 11°$). 1749+701: A sugggestion of intermediate time-lag plateau at 8.0 and 4.8 GHz, perhaps associated with extrinsic variability ($b \sim 31°$). 3C 371: Flat—consistent with an uncorrelated stationary process. OV−198: Hopelessly noisy at 4.8 GHz; poorly defined at 14.5 and 8.0 GHz. 2005+403: A suggestion of intermediate time-lag plateau at 8.0 and 4.8 GHz, perhaps associated with extrinsic variability ($b \sim 4°$) (see Spangler et al. 1988). 3C 418: Too noisy to extract any values: 2131−021: Poorly defined, and gradual turnover makes time-scale estimate uncertain. 2134+004 Poorly defined. BL Lac: Gradual turnover makes time-scale estimate uncertain. CTA 102: Poorly defined plateau.

TABLE 4

TWO-SAMPLE TESTS FOR BL LAC OBJECTS AND QSOs: TOTAL FLUX

Test	Time Scales	Slopes (all)	Slopes ($0 < b_S < 1.5$)
Gehan's Generalized Wilcoxon	0.79	0.13	0.40
Logrank	0.96	0.11	0.27
Cox-Mantel	0.96	0.09	0.26
Peto & Peto Generalized Wilcoxon	0.82	0.13	0.40

TABLE 5

STRUCTURE FUNCTION SLOPES: TOTAL FLUX

Subset	Slopes (b_S)
All sources	1.09 ± 0.34
BL Lac objects: all	0.94 ± 0.37
BL Lac objects $b_S > 0$	1.05 ± 0.20
QSOs: all	1.18 ± 0.28
QSOs: $b_S < 1.5$	1.04 ± 0.18

power-law portion of the structure function of a purely random noise process), the time scales for the QSO set will have been underestimated. Our data are therefore consistent with QSOs having on average a somewhat longer characteristic time scale. However, in view of the slight difference we have found, in the following correlation analyses we do not subdivide sources by type.

We have analyzed these data in an attempt to find correlations, both between the measured values, and with other relevant parameters;[1] our motivation for the choice of parameters and our conclusions are presented in § 4. Figures 4*a*–4*c* and Table 6 show our attempt to correlate time scale with redshift, slope, 14.5 GHz variability, 4.8 GHz variability, power in extended structure, and compactness. The smaller the value in Table 6, the stronger the evidence of correlation. The four estimates are by the two correlation utilities in ASURV, first for time-variable values, and then for log (time)-log (variable) values. The numbers in each column are generally similar, which gives us some confidence in them. Each of these methods allowed us to incorporate the fact that some of our time scales are lower limits.

A depressingly small fraction of the BL Lac objects have redshifts, and as these are needed for generating an estimate of the source luminosity, we have assigned a redshift to BL Lac objects where none exists, by using the mean redshift ($z = 0.475$) of those in the sample that are known. Table 6 shows that we find no correlation between redshift and time scale. In principle, time scales need to be transformed into "source frame" values using a $(1 + z)$ factor; however, given our inadequate knowledge of redshifts, the fact that (unknown) intrinsic beaming is likely to be a more important effect, and that no correlation exists between time scale and redshift, we have not applied this "correction." [We have confirmed that there is no significant correlation between z and $t/(1 + z)$.]

The statistics suggest a correlation of time scale with slope significant at the few percent level; and the eye of faith may see this trend for slope to increase with time scale in Figure 4*a*. As sources with steep slope are preferentially QSOs, this is further (albeit weak) evidence that QSOs have somewhat longer characteristic time scales than do BL Lac objects.

We have computed variability indices [defined by $(S_{\max} - S_{\min})/(S_{\max} + S_{\min})$; e.g., Aller, Aller, & Hughes 1991a] at 14.5 and 4.8 GHz, and the former is plotted against time scale in Figure 4*b*. A very weak correlation is possible at 14.5 GHz, with no significant correlation at 4.8 GHz (see also Table 6). A trend for the variability to be lower at long time scales might be expected because at long time scales we are observing sources whose extrema of variation are yet to be detected. This draws attention to the fact that some of our time scales (not just those we have assessed as lower limits, but also some with poorly defined plateaus, that may prove to have more extended power-law regions when data spanning a greater time-lag range are available) may be underestimated, and as this applies preferentially to QSOs, again we have a suggestion that QSO time scales might be somewhat longer than those of BL Lac objects.

We have estimated the power in extended structure from the flux density at 365 MHz, by converting to a rest frame spectral luminosity (in arbitrary units) using a spectral index $\alpha = 0.5$ and $q_0 = 0.5$:

$$\mathscr{L} \propto S_{365} R_a^2 (1 + z)^{(3+\alpha)} \quad (1)$$

where the angular size distance measure is

$$R_a = z[(1 + \sqrt{1 + 2q_0 z} + z)/(1 + \sqrt{1 + 2q_0 z} + q_0 z)]/(1 + z)^2 . \quad (2)$$

[1] We have performed no regression analyses, for several reasons: First, what trends we do find are very weak. Second, "common" methods (e.g., χ^2 and M-estimates) do not allow us to incorporate our lower limits. The packet ASURV provides methods for incorporating lower limits, but, in general, only on the dependent variable. We can treat time as the dependent variable, but a regression analysis of time on "other variable" is of little interest. The Schmitt method allows "censoring" of the independent variable, but the derived coefficients depend sensitively on the user's choice of binning—and we have no check on the results from other techniques.

TABLE 6

CORRELATIONS FOR τ_S

Statistic	Redshift	Slope	14.5 GHz Variability	4.8 GHz Variability	Extended Power	Compactness
Probability[a]	0.72	0.05	0.15	0.21	0.95	0.02
Probability[b]	0.90	0.02	0.09	0.26	0.21	0.01
Probability[c]	0.89	0.06	0.18	0.29	0.56	0.06
Probability[d]	0.90	0.02	0.09	0.26	0.21	0.01

[a] Measure of correlation using Cox Proportional Hazard model; time-variable plane.
[b] Measure of correlation using Generalized Kendall's Tau method; time-variable plane.
[c] Measure of correlation using Cox Proportional Hazard model; log (time)-log (variable) plane.
[d] Measure of correlation using Generalized Kendall's Tau method; log (time)-log (variable) plane.

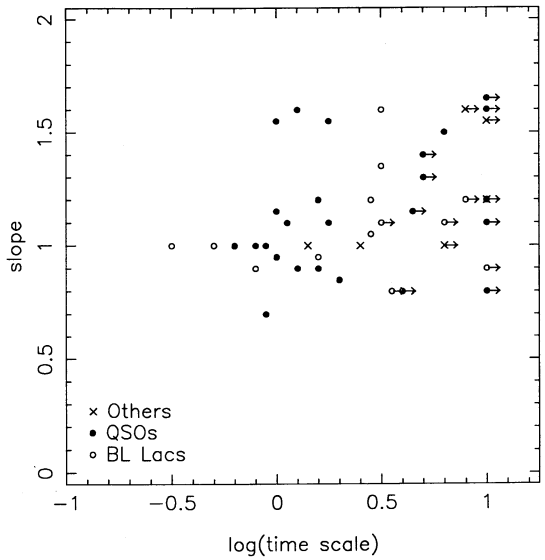

FIG. 4a

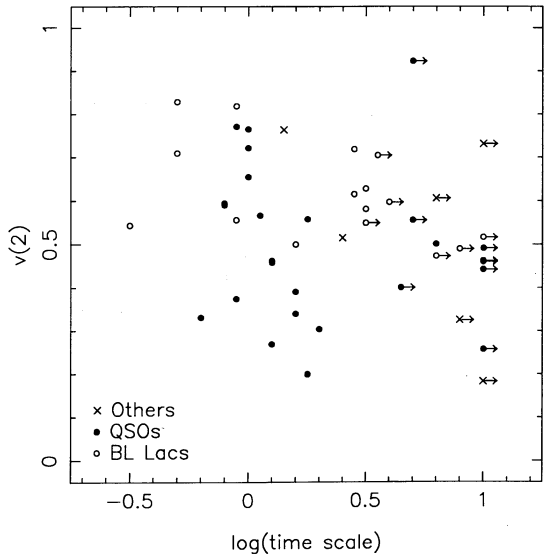

FIG. 4b

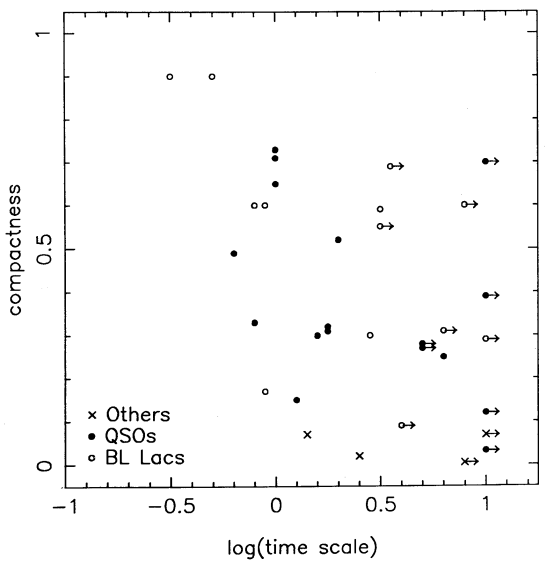

FIG. 4c

FIG. 4.—(*a*) Derived slope vs. derived characteristic time scale. (*b*) Variability index (derived as described in the text) at 14.5 GHz vs. characteristic time scale. (*c*) Compactness, as measured by a visibility function, vs. characteristic time scale.

Flux data have been obtaned from various references, interpolating or extrapolating to 365 MHz if necessary. To estimate compactness we have used the visibilities of Preston et al. (1985). This restricts the number of sources for which we have an estimate of compactness, but while other estimates of compactness exist (e.g., Pearson & Readhead 1988; Antonucci & Ulvestad 1985), where they overlap, the values are so discrepant that we were reluctant to use a more heterogeneous set. Table 6 shows that we find no correlation between power in extended structure and time scale. This is not entirely surprising: our method of estimation is valid only if all sources have the same volume, spectral slope, and age. Furthermore, the 365 MHz flux—although dominated by extended emission in many sources—may well be contaminated by core emission in some sources. A lot of scatter is thus to be expected. Figure 4*c* and Table 6 indicate a possible weak correlation, the sources with longer time scales being those with smaller "compactness"—that is, they have relatively more power in extended structure.

3. STRUCTURE FUNCTION ANALYSIS OF THE POLARIZED FLUX

We have applied a structure function analysis similar to that described above to the polarized flux variations seen in the UMRAO monitoring data. The integrated polarized flux itself is not a good diagnostic of the conditions in the emitting region, because subregions of orthogonally polarized emission may cancel to produce a null in the overall polarization, while each element of the flow is significantly polarized. The distinct regions will be evident in the variability exhibited in Q and U, however, and so working with these parameters provides more information about the source behavior. The Q and U values are normally defined with respect to Earth's celestial coordinate system. In order to make these values more physically meaningful, we have rotated the $Q-U$ plane so that Q is positive if the electric vector lies along the direction of the VLBI jet *when that is known.* Thus fluctuations in an E-vector parallel (or perpendicular) to the flow will contribute only to Q. The position angles of VLBI jets that we adopted from the literature and used in this analysis are listed in Table 2. The list is by no means complete, and there are numerous cases where the values is uncertain: structure may be complex, may exhibit bends and may be frequency- and/or resolution-dependent. We have determined values by reference to the original maps where possible; and where these are not available we have adopted quoted values dislaying broad agreement between different authors, ignoring apparently "discrepant" estimates. Nevertheless, we suspect that uncertainties in the determination of the structure PAs lead to considerable "noise" in our results. Rotation measures are known for the majority of sources, and we have performed a frequency-dependent derotation on Q and U using the values listed in Table 2. For most

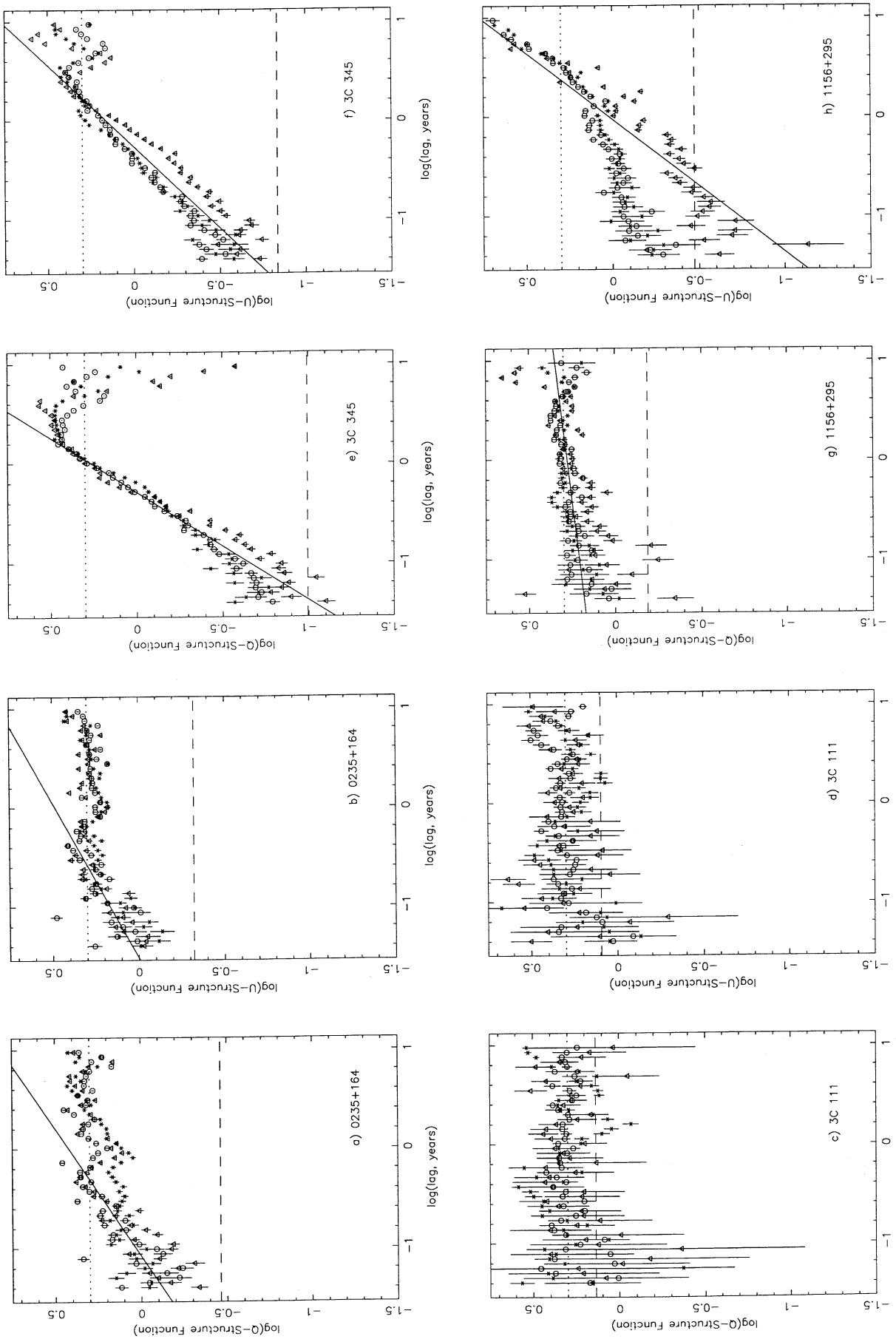

FIG. 5.—Examples of the structure functions for polarized flux variations. Q structure functions are shown on the left, and U structure functions on the right of each pair. Triangles denote 4.8 GHz observations, circles are 8 GHz observations, and crosses are 14.5 GHz observations. The short-dashed horizontal line shows the anticipated long time-lag plateau (having normalized the function with the variance, σ^2, at each frequency), and the solid line is our estimate of the slope in the power law portion of the curve. The long-dashed horizontal line indicates the anticipated contribution from measurement error.

sources the rotation measure is small and the derotation has little effect at centimeter wavelengths. This means that uncertainty in the value of the rotation measure, and the absence of a value for about 20% of the sources, should not have a significant influence on our results.

Variations of the polarized flux are generally shorter in time scale than those of the total flux and thus occur nearer to the limit of our time resolution; furthermore, the signal-to-noise is not as good for the polarized flux which is on the order of a few percent of the total flux. For these reasons the Q and U structure functions are not as well defined as those for the total flux. Examples are shown in Figures 5*a*–5*h*. Figures 5*a*–5*b* show a typical pair of Q and U structure functions. The Q and U curves are similar; both display a reasonably clear power-law portion and plateau at the anticipated value of 2 σ^2. The power-law portion is, however, much shallower than that seen in the total flux curves. There is a dispersion in slopes, so that some sources (e.g., 3C 111; Figs. 5*c*–5*d*) have almost flat structure functions, while a few (e.g., 3C 345; Fig. 5*e*–5*f*) have steeper slope—a value closer to ~ 1.0 as found for the total flux. A small subset of sources displays quite different Q and U structure functions (e.g., 1156+295; Figs. 5*g*–5*h*). The quasar 1156+295 also serves to demonstrate features that are quite common: in Q we see the "hint" of a power-law portion at very short time lag; we have used such trends to estimate a time scale when this is all that is available. In U we see no plateau at long time lag, and here we assume that the longest time lag sets a lower limit to the characteristic time scale. As with the total flux structure functions, a long-dashed line indicates the anticipated contribution from the signal noise, and here also, we have not subtracted this contribution. We note that this cannot explain the shallow slopes evident in many Q and U structure functions: failure to remove a constant base-level D^b contribution to a "true" signal D will lead to an underestimate of the slope from a measure in the $\log D - \log \tau$ plane between τ_l and τ_u of $[\log (1 + [D_l^b/D_l]) - \log (1 + [D_u^b/D_u])]/\log (\tau_u/\tau_l)$. For our range of τ and estimated power laws for the Q and U structure functions, and given that where ever a well-defined slope is evident, $D(\tau_l) \gtrsim D^b(\tau_l)$, the error can be no more than ~ 0.15 (and this will be evident only as a flattening at short time lag). Given the mean and dispersion of the derived slopes, this is not significant.

We have estimated slopes and characteristic time scales as for the total flux case, and the values we derive are listed in Table 3. There are numerous cases where we feel unable to estimate a time scale; in most cases we can estimate a slope, but it is not always clear that we are making a measurement on the "true" power-law portion of the curve: in particular, we may be including values $b_{Q,U} \sim 0$ by virtue of inadvertently measuring an ill-defined plateau. Figures 6*a*–6*b* show plots of slope and time scale derived from Q and U independently. The strong trend for points to lie along the line of unit slope is a visual indicator that, despite the above mentioned limitations, we can have some confidence in our derived values.

3.1. *Time Scales and Slopes*

The distributions of time scales and slopes are shown in Figures 7*a*–7*d*. Lower limits have been plotted as actual values. Figures 7*a*–7*b* show the distribution of time scales for both Q and U. To casual inspection it is not clear whether the distribution of time scales in Q is significantly different for BL Lac objects and QSOs. We have performed the same two-sample tests discussed for the total flux, and the results are summarized in Table 7. It can be seen that there is a 30%–50% probability that the BL Lac and QSO distributions of τ_Q are drawn from the same population (i.e., there is no strong indication that they are from different populations). Inspection of Figure 7*b*, however, strongly suggests that in U the BL Lac objects typically have a much shorter time scale compared to the QSOs. This is also suggested by the two-sample tests (Table 7) that show a probability of only a few percent that the BL Lac objects and QSOs are from the same population. Figures 7*c*–7*d* show the distribution of slopes for Q and U: as with those derived for a total flux, they form a quite narrow distribution (indeed, the spread is only slightly greater than for

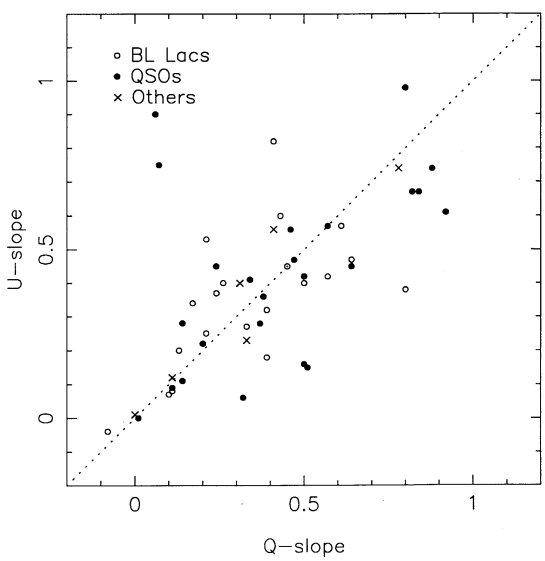

FIG. 6*a*

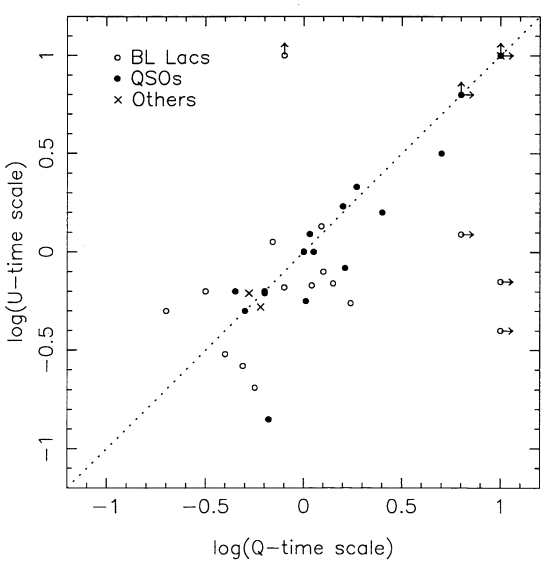

FIG. 6*b*

FIG. 6.—(*a*) Comparison between power-law slopes derived independently from Q and from U structure functions. The dotted line has unit slope. (*b*) Comparison between time scales derived independently from Q and from U structure functions. The dotted line has unit slope.

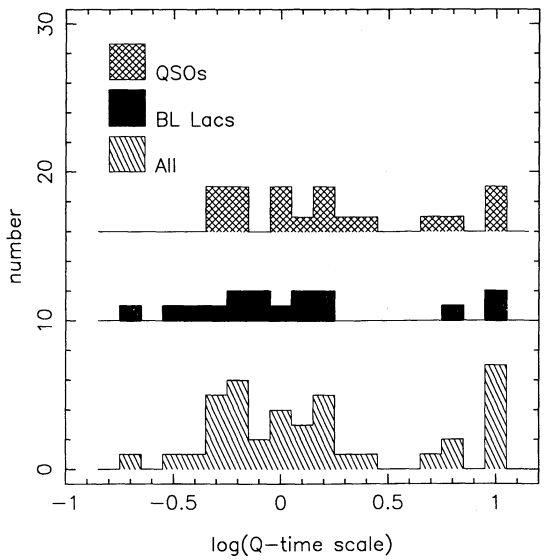

FIG. 7a

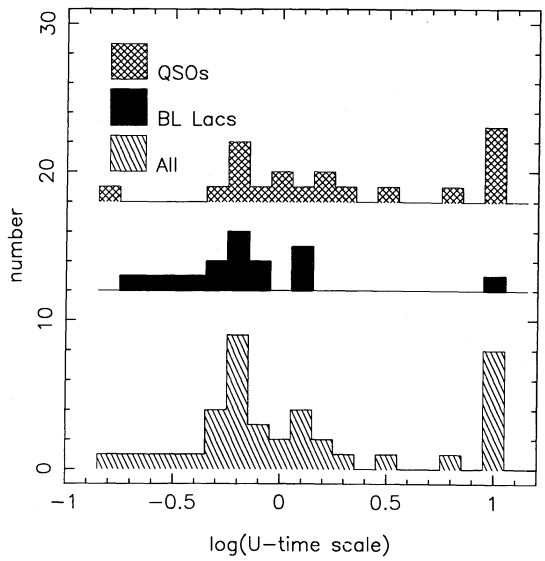

FIG. 7b

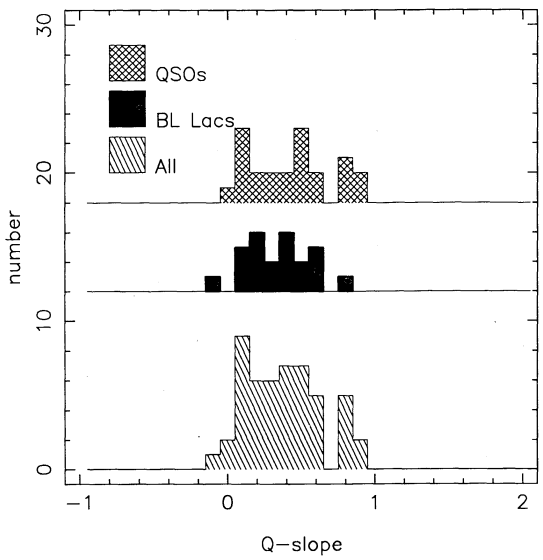

FIG. 7c

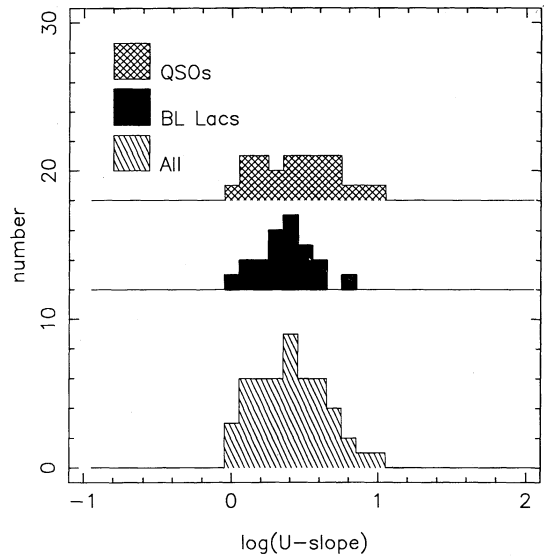

FIG. 7d

FIG. 7.—(*a*) Distribution of characteristic time scales estimated from the Q structure functions for all surces in the sample, BL Lac objects, and QSOs. (*b*) Distribution of characteristic time scales estimated from the U structure functions for all sources in the sample, BL Lac objects, and QSOs. (*c*) Distribution of slopes estimated from the Q structure functions for all sources, BL Lac objects, and QSOs. (*d*) Distribution of slopes estimated from the U structure functions for all sources, BL Lac objects and QSOs.

the total flux slopes; compare values in Table 5 with those in Table 8), but, rather strikingly, *at a much lower mean value* than that of the total flux slopes. Applying the same statistical analysis to the slopes, we find no compelling evidence that the BL Lac and QSO slopes are from different parent populations, in agreement with the result for the total flux structure function slopes.

Mean values of these distributions (using the actual values of lower limits where necessary; and including values for the total flux time scales for comparison) are given in Table 8. The difference in mean characteristic time scale for BL Lac objects and QSOs derived from the total flux displays the weak tendency for BL Lac objects to have a shorter time scale of variation—as noted above. It will also be seen that for both BL Lac objects and QSOs the time scale for variations in Q is 60%–70% shorter than that for the total flux variations. This is consistent with the interpretation of these variations in terms of shocks whereby the total flux increases as a shock passes from the optically thick to the optically thin portion of the flow, but is lagged by the increase in the polarized emission because of suppression of the latter by Faraday effects, even when the opacity is low (Hughes, et al. 1989a). This would lead to a somewhat lower "lower limit" to the range of response time scales for Q as compared with I, as discussed in § 2.1. For QSOs a similar reduction may be seen in the U time scales. However, for BL Lacs the mean U time scale is only one-third

TABLE 7

TWO-SAMPLE TESTS FOR BL LAC OBJECTS AND QSOS: POLARIZED FLUX

Test	τ_Q	τ_U	b_Q	b_U
Gehan's Generalized Wilcoxon	0.31	0.02	0.39	0.32
Logrank	0.47	0.02	0.16	0.15
Cox-Mantel	0.47	0.01	0.14	0.13
Peto & Peto Generalized Wilcoxon	0.31	0.02	0.39	0.32

TABLE 8

MEAN VALUES OF SLOPES AND TIME SCALES

Parameter	All	BL Lac Objects	QSOs
$\langle b_Q \rangle$	0.38 ± 0.25	...	...
$\langle b_U \rangle$	0.39 ± 0.24	...	...
$\langle \log(\tau_Q) \rangle$	...	0.06 ± 0.49	0.22 ± 0.44
$\langle \log(\tau_U) \rangle$	...	-0.15 ± 0.37	0.25 ± 0.54
$\langle \log(\tau_S) \rangle$	...	0.29 ± 0.42	0.37 ± 0.41

that of the total flux time scale (as noted above in connection with the two-sample tests for BL Lac and QSO values of τ_U). We discuss the implication of this result in the next section.

Plots of log (τ_Q) and log (τ_U) versus log (τ_S) are shown in Figures 8*a*–8*b*, and the correlation statistics relating to these plots are given in Table 9. The correlations are reasonable, and it is no surprise that there is not less than a 5%–10% probability of a lack of correlation, given the dispersion that has probably been introduced by our limited ability to orient Q with the jet direction (see above), and the fact that the polarized flux time scales, being short, and close to our limit of time resolution, cluster in the log $(\tau_{Q,U})$–log (τ_S) plane.

Figures 9*a*–9*b* show plots of log (σ_Q^2/σ_U^2) versus log (τ_S) for observing frequencies of 4.8 and 14.5 GHz. If all source variations are associated with axial shocks, so that the variations contribute only to Q (in our chosen reference frame), we might expect the observed variations in Q to be greater than those in U—the latter being "contamination" because of our inability to correctly align Q with the direction of the VLBI jet in some cases. It is possible that, as a significant number of sources exhibit a long characteristic time scale, in some sources we have not seen the full range of amplitudes of variation and have underestimated the dispersion: as the U variations have a shorter time scale, we would have underestimated the Q dispersion with respect to the U dispersion. If so, we would expect the ratio of dispersions to correlate with time scale—the value of σ_Q^2/σ_U^2 being higher for shorter τ_S, for at shorter time scales we will have more adequately sampled the full range of fluctuations. There is no discernible trend at 4.8 GHz (Fig. 9*a*), and—to the extent that there is a hint of a trend in Figure 9*b*—it is counter to that anticipated. The internal scatter and frequency-dependent effects completely mask any sampling effect—suggesting that it must be small. We are therefore left with the conclusion that the Q and U dispersions are comparable, which appears inconsistent with our simple picture of the fluctuations being due to jet shocks. We believe that this is related to the different time-scale distributions for Q and U and discuss in the next section how these results may be explained within the shocked-jet scenario.

Figures 7*c*–7*d* and the values in Table 8 show that the slopes in both Q and U are very similar, and, in general, lower than for the total flux. It is tempting to speculate that this arises largely from "confusion": if the Q and U variations have the character of "shot noise," as for the total flux, but the associated power-law portion of the polarized flux structure functions is not evident in consequence of the narrow time-lag range of correlated fluctuations available to us (minimum and maximum characteristic time scales so close together that the transition regions merge), it is easy to see that we might inadvertently measure a shallower slope than the one that would otherwise be found. In this case, we would expect a strong correlation between slope and time scale—the higher the char-

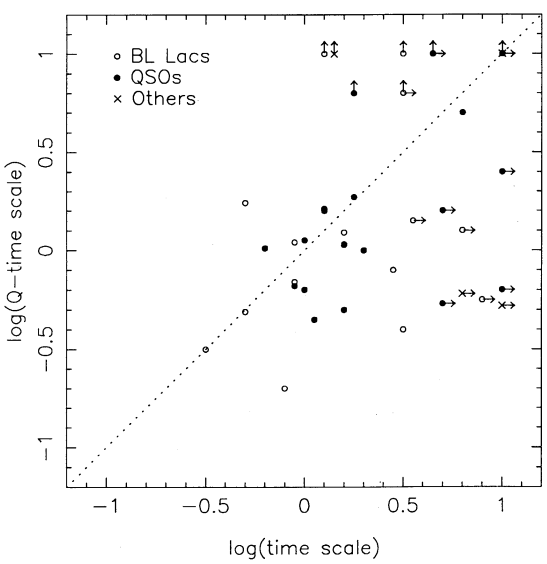

FIG. 8*a*

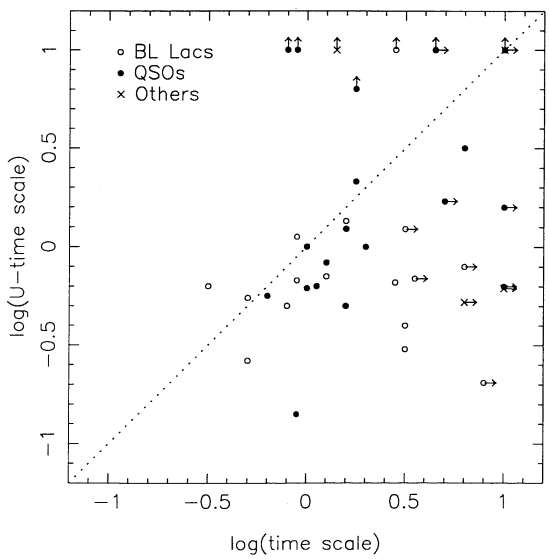

FIG. 8*b*

FIG. 8.—(*a*) Comparison of the characteristic time scales derived from the Q structure function with those derived from the total flux structure functions. The dotted line has unit slope. (*b*) Comparison of the characteristic time scales derived from the U structure function with those derived from the total flux structure functions. The dotted line has unit slope.

TABLE 9

CORRELATIONS FOR TIMES AND SLOPES

Statistic	log (τ) vs. log (τ_Q)	log (τ) vs. log (τ_U)	b_Q vs. log (τ_Q)	b_U vs. log (τ_U)
Probability[a]	...	...	0.01	0.005
Probability[b]	0.05	0.10	0.005	0.02

[a] Measure of correlation using Cox Proportional Hazard model.
[b] Measure of correlation using Generalized Kendall's Tau method. This admits lower limits on both variables.

acteristic time scale, the more accurately should we be able to estimate a slope $O(1)$. This is apparent in both Figures 10*a*–10*b* and the correlation probabilities in Table 9: longer time scales seem to be associated with an approach to $b \sim 1$, and the correlation is seen from the statistics to be significant. If this is the correct explanation for the values of the Q and U slopes, it seems slightly odd that they would cluster so tightly about a value $\lesssim 0.4$. The latter point provides some evidence that the polarized flux structure functions have slopes significantly shallower than do the total flux structure functions. We are, however, unable to suggest *why* this might be the case.

4. DISCUSSION

It is possible that longer characteristic time scales arise from greater source size: Wehrle et al. (1991) have found evidence that compact steep spectrum quasars are larger than flat spectrum quasars which, in turn, are larger than BL Lac objects; from a sample of four BL Lac objects, the latter are found to be only one-quarter the size of the CSS quasars. However, the dispersion of our time scales within classes is much larger than the difference in this dispersion between classes—unlike the distribution of length scales. This suggests that the wide spread in time scales is not set by length scales, but is caused by a mechanism that exhibits a large intrinsic dispersion and is not very different from QSOs to BL Lac Objects. (Note that our measured time scales are *maximum* time scales; a minimum time scale will be set by the physical size of an emitting region, which in general will be smaller than the length scale of the region through which this emitting element propagates.) Evidence is mounting that BL Lac objects and radio-loud QSOs are populations related to FR I and FR II sources, respectively (Bregman 1990); and the two FR classes each span a wide range of energies. The difference in morphology between FR I and FR II sources is conventionally explained as due to the former being less energetic and hence less stable: is the stability of the flow the factor that determines the distribution of time scales? If a more energetic flow is more stable, and so exhibits variations that remain correlated over longer time scales, we might expect a correlation between time scale and a measure of the overall source energetics. Possible measures of the source energetics are luminosity in extended structure and compactness. These possibilities motivated the exploration of correlations described in § 2.2.1.

The lobe luminosity can be expected to measure the energy deposited by the flow over the source's lifetime, and will be greater, the more energetic the flow; furthermore, it is believed to be free of any Doppler boosting. Again by analogy with FR radio sources, we anticipate that the more stable the flow, the more energy is deposited in—and so is emitted by—a non-Doppler-boosted lobe, than by the jet that feeds it. As shown in § 2.2.1 we found no correlation between time scales and an estimate of the lobe luminosity, although, as noted, there is considerable uncertainty in our estimate of the latter.

It might be argued that a link between compactness and time scale merely confirms that smaller structures vary more rapidly. However, we have already noted above that it is difficult to forge a link between time scale and size. A greater fraction of the total flux within an unresolved core can imply more flux within a fixed fraction of the source volume and not necessarily a smaller length scale containing a fixed fraction of the flux. The compactness may then measure the efficiency with

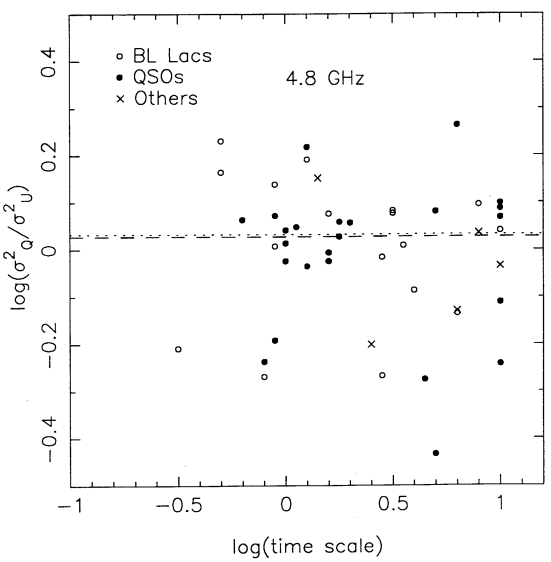

FIG. 9*a*

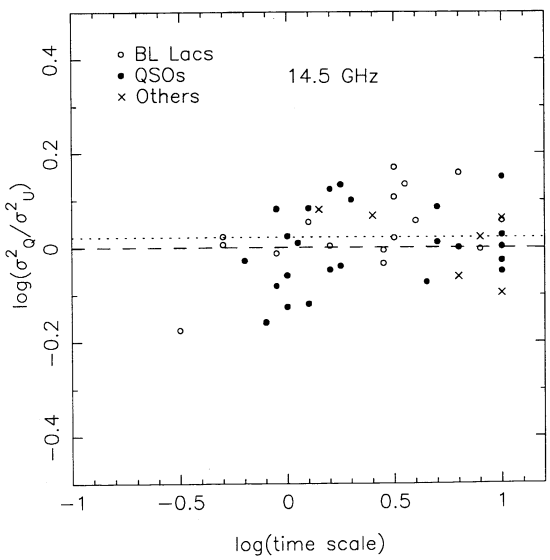

FIG. 9*b*

FIG. 9.—(*a*) Values of the ratio of the Q and U variances for all sources in the sample, at an observing frequency of 4.8 GHz. The dashed horizontal line is the median of log (σ_Q^2/σ_U^2) for BL Lac objects, and the broken line is this value for the QSOs. (*b*) Values of the ratio of the Q and U variances for all sources in the sample, at an observing frequency of 14.5 GHz. The horizontal lines are as for Fig. 9*a*.

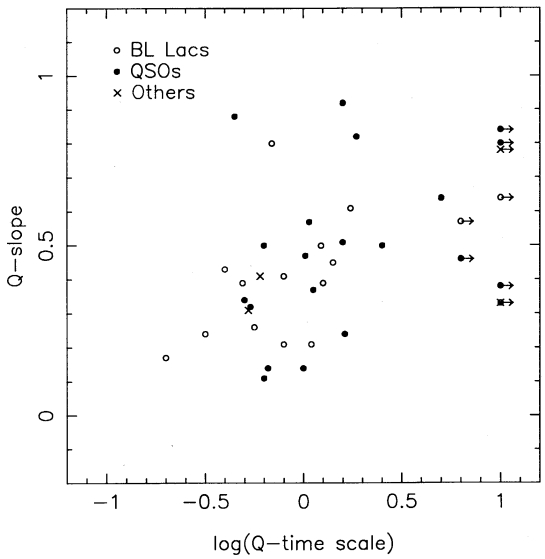

FIG. 10*a*

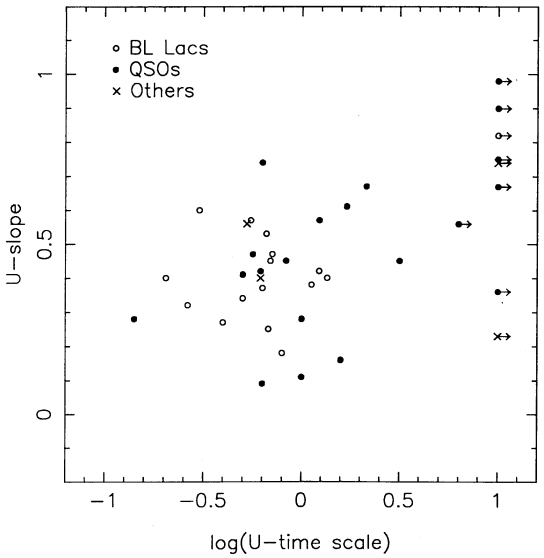

FIG. 10*b*

FIG. 10.—(*a*) Comparison of the slopes with the characteristic time scales derived from the Q structure function. (*b*) Comparison of the slopes with the characteristic time scales derived from the U structure function.

which energy is transported to large-scale structure, and so *may* reflect the global energetics, and hence the stability of the flow. An anticorrelation between time scale and compactness (low values implying power in extended structure) would then be circumstantial evidence that time scales were determined by flow stability. As found in § 2.2.1, there is a very weak trend evident in the compactness data, which is not inconsistent with our expectations.

Numerous other factors may influence time scales, and many of these may be expected to show a frequency dependence: A dispersion in magnetic field strength, particle density, and physical scale among sources will lead to a dispersion in opacity at a given observing frequency, and hence to a dispersion in volumes from which emission is seen. Correspondingly, this volume will change with frequency. Events associated with a smaller volume would be expected to display shorter time-scale behavior. Further, if variability is indeed associated with shocks, then the shock volume will be frequency dependent (Marscher & Gear 1985), and the outburst decay time may also be frequency dependent—if at some frequency the shock width is much less than the visible portion of the jet, but much longer than the visible jet at another frequency. This is not true of propagating "blobs" of plasma (which are not delimited on one side by a plane at which energization occurs), and so a frequency dependence of time scales provides a method of distinguishing between causes of variability. We found that the total flux structure functions exhibited little frequency dependence (see Fig. 2), in either their slope or time scale of plateauing. This may well reflect the rather narrow range of frequencies considered in this analysis, and a comparison of our results with structure functions of significantly higher frequency data is desirable.

Another possibility is that the spread in time scales that we see is of "extrinsic" rather than of "intrinsic" origin: it might simply reflect the spread in Doppler factors, transforming a single rest frame time scale. Consider an ensemble of sources with flow speed γ and intrinsic time scale t'. If they are randomly aligned in space so that the number oriented between Ψ and $\Psi + d\Psi$ from our line of sight is $dn' = n'_\Psi\, d\Psi = n(t)dt$, where n'_Ψ is a constant, and we see $n(t)dt$ in the interval dt because of the distribution in $t = \mathscr{D}^{-1}(\Psi)t'$, the differential number distribution is

$$n(\hat{t}) = \frac{n'_\Psi}{t'\sqrt{2\gamma\hat{t} - 1 - \hat{t}^2}} \tag{3}$$

where $\hat{t} = t/t'$ satisfies

$$\gamma - \sqrt{\gamma^2 - 1} < \hat{t} < \gamma + \sqrt{\gamma^2 - 1}\,. \tag{4}$$

(This may be compared with the distribution of velocities, e.g., Cawthorne 1991.) If we associate the upper and lower limits of our observed time-scale distributions with the limits on $\hat{t}$, we have

$$t_{\min}/t' = \gamma - \sqrt{\gamma^2 - 1}\,, \tag{5a}$$

$$t_{\max}/t' = \gamma + \sqrt{\gamma^2 - 1}\,, \tag{5b}$$

from which we can estimate both t' and γ. The minimum time scale is $\sim\frac{1}{3}$ yr, while the maximum that we find is ~ 10 yr. These numbers imply that $\gamma \sim 3$ at $t' \sim 1.5$ yr. Now it is unlikely that every source has the same γ, and even less likely that they are randomly oriented in space: on the basis if received wisdom we would contend that we select sources beamed toward us. Furthermore, if short time scales result from large values of $\mathscr{D}$, there should be a stronger correlation between time scales and other parameters: for example, variability index, which is sensitive to observing frequency, and hence Doppler factor. We have already noted the depressingly weak tendency for time scales to correlate with anything! However, the above does illustrate that it is not difficult to obtain the sort of dispersion in time scales that we see, simply from an orientation-related dispersion in Doppler factors, and this should be borne in mind when interpreting these results.

In § 3 we noted that the U time scales were distinctly shorter than the Q times scales for BL Lac objects, but not for QSOs; and that the ratio of dispersions in Q and U is of order one for

both types of source. One possible explanation for these results within the shocked-jet scenario is as follows: For BL Lac objects there is a strong correlation between the magnetic field alignment of propagating components and the jet axis (Gabuzda & Cawthorne 1991). Such events, being fairly long-lived, will tend to populate the longer time-scale region of the Q time-scale histogram and lead to large values of σ_Q^2/σ_U^2. However, the core contributes a nonnegligible fraction of the integrated emission in many objects (Gabuzda et al. 1992): although relatively weakly polarized, the core is bright, and the polarized flux from the core is usually within an order of magnitude of that from the jet. However, the orientation of the polarization vector of the core flux is essentially random. The reason for this is unknown, but within the shocked-jet scenario it could be explained as either the Faraday rotation of a constant intrinsic alignment, or the real bending of an unresolved jet within which the magnetic field characterizes the instantaneous flow direction. In either case, the core fluctuations are of shorter time scale—probably because of the smaller length scale—and of comparable magnitude in Q and in U. When the core fluctuations dominate the integrated emission, they add a significant population of points to the shorter time-scale region of both the U and the Q time-scale histograms and "contaminate" the σ_Q^2/σ_U^2 plot with many values of order unity. For QSOs the situation is somewhat different, as their cores are essentially unpolarized. However, although there is a tendency for the propagating components to have magnetic field aligned parallel to the jet, this correlation is far less strong than the corresponding tendency for BL Lac objects to have perpendicular field components (Gabuzda & Cawthorne 1991). In this case, the comparable Q and U time-scale distributions and dispersion arise from an effect intrinsic to the flow. It remains unclear how the shocked-jet model applies to these objects, although it seems reasonable to suppose that the mean axial field is stronger and is the main determinant of the position angle of the polarized flux, even after the shock amplification of the turbulent component.

U contributions might come from oblique shocks, but that would not explain a difference in time scales: BL Lac objects might exhibit shorter characteristic time scales than QSOs, but if we were seeing the results of a dispersion in shock orientation, there is no obvious reason why the U variations should not have the same distribution of time scales as the Q variations. Another possibility is that in U we are seeing an independent mode of variation (more akin to turbulence) that has a short characteristic time scale for BL Lac objects, and a longer characteristic time scale—comparable to that of the shock induced Q variations—for QSOs because of their greater power, and hence stability (as noted above). For BL Lac objects this would lead to population of the short time-scale portion of the time-scale historgrams, with the long time-scale portion of the Q time-scale histogram being filled in by sources wherein shocks dominate the behavior. If there are two origins to the observed fluctuations, although we might not expect to see any particular value of σ_Q^2/σ_U^2, an approximate equipartition of energy is plausible. Local enhancements of density and magnetic field that contribute to U variations are likely to be of the same order of magnitude as those that form shocks and contribute to Q variations. Indeed, the U fluctuations might be due to a highly time-variable downsteam flow, as is often observed in Earth's bow shock (Eilek & Hughes 1991). In this case, $(\sigma_Q^2/\sigma_U^2) \sim 1$ is to be expected. Nevertheless, while such possibilities should be borne in mind, we consider that, as argued above, the results of our analysis are consistent with a simple shocked-jet model.

Numerous claims for the existence of periodic behavior have been made in the literature: e.g., Barbieri et al. (1990) for 3C 446, Valtonen et al. (1988) for OJ 287. Such behavior is usually claimed on the basis of optical monitoring and is plausibly associated with an accretion structure or massive binary system. It seems very unlikely that radio emission—which is observed predominantly from the parsec-scale structure—would exhibit any harmonic variations, although a "regularity" is certainly not out of the question. The latter possibility and the recent evidence for a link between radio and optical variability (Quirrenbach et al. 1991) do make it desirable to search for evidence of periodicity, despite the aforementioned prejudice against finding it. To this end we have used conventional periodogram analyses (Deeming 1975; Scargle 1982) and maximum entropy spectral methods (e.g., Haykin & Kesler 1979; Ulrych & Ooe 1979) on the time series for which we have computed structure functions. None of these methods are wholly satisfactory: The conventional periodogram has much structure associated with the time series "window." The problem with the maximum entropy method is that of choosing the optimum number of "poles": too few, and the periodogram is smooth, and no individual peaks are evident; too many and spurious structure develops—but since one does not know a priori what structure one is to see, one cannot judge easily what structure is spurious. What structure we find in the periodograms appears to be simply related to the data window, with the possible exception of a periodicity of ~ 1.67 yr in the source OJ 287 (see Aller et al. 1991b). Nevertheless, for completeness, we plan to use the CLEANED periodogram (Roberts, Lehár, & Dreher 1987) in an attempt to confirm our results—which to date are that no significant periodicity is evident in the UMRAO data.

The appeal for "more data" is a common one, but we believe the above analyses demonstrate that in two respects the acquisition of more data would be valuable. It is evident that the current time span is insufficient to define clearly the structure function plateau in a significant number of sources, and that some years more monitoring data will give us both better defined time scales and time scales for more sources (as the data base for those sources for which monitoring started only recently is increased). Equally importantly, it is evident that we need monitoring on a time scale of weeks to days: only then will we be able to define adequately the character of the short time-scale variations in polarized flux, and its dependence on source type. Such monitoring is also essential for probing the link between the monthly—yearly flux variations evident in the UMRAO data base, and the rapid variability that appears to be a feature in many objects (e.g., Quirrenbach et al. 1991).

The total flux structure functions for both BL Lac objects and QSOs in our sample generally conform to the "ideal" expected for a stationary random process plus measurement noise. Both classes of object exhibit a power-law slope $b \sim 1$, indicative of "shot" or "random walk" noise at high frequency. This does not tell us the underlying physical mechanism for the variations, but implies that in both types of object we are seeing the result of slowly decaying responses to white-noise impulses. The characteristic time scales for BL Lac objects may be slightly shorter than those for QSOs, but both are of the same order of magnitude, and both exhibit a wide range of values. These results are in general agreement with those of Bregman et al. (1988), for example, where radio fre-

quency emission was found to exhibit a structure function slope $b \sim 1$ (steeper than that at optical frequencies for the same source), and with those of Fiedler et al. (1987), showing a broad range of slopes and characteristic time scales similar to those found here. Given the success of the shocked-jet model for several well-defined outbursts in BL Lac, 3C 279 and OT 081, we feel that the current work provides good circumstantial evidence for the general validity of this model.

The polarized flux structure functions have relatively shallow slopes, and we have not been able to demonstrate conclusively whether this is an intrinsic effect, or merely a consequence of our limited time resolution and signal-to-noise for the polarized flux. Despite this, we are able to get reasonable estimates of the characteristic time scales for variations of the polarized flux, and we find that these are somewhat less than the corresponding time scales for the total flux: this result is expected of a scenario in which slugs of plasma (shocks?) propagate from an opaque to the transparent region of a source, with opacity and Faraday effects suppressing the polarized emission at the onset of the total flux "event."

The most distinctive feature of the Q and the U time scales is that for BL Lac objects the U distribution is skewed toward low values compared with both the Q distribution, and the Q and the U distributions for QSOs. Furthermore, for both classes of source $\sigma_Q^2/\sigma_U^2 \sim 1$. We have argued that, although these results might be taken to imply the existence of a contribution to the variability that is quite different to that associated with shocks, these results can be understood in the context of the shocked-jet scenario if allowance is made for the contribution to the integrated emission from the core in BL Lac objects, and for the nature of the jet magnetic field configuration in QSOs.

We wish to thank Joel Bregman for supplying us with the source code for the ASURV package and John Wardle and Denise Gabuzda for many useful comments that helped us improve the presentation of this study. This work was supported in part by grant AST-8815678 from the National Science Foundation.

REFERENCES

Aller, H. D., Aller, M. F., Latimer, G. E., & Hodge, P. E. 1985, ApJS, 59, 513
Aller, M. F., Aller, H. D., & Hughes, P. A. 1991a, in Variability of Active Galactic Nuclei, ed. H. R. Miller & P. J. Wiita (Cambridge: Cambridge Univ. Press), 184
Aller, M. F., Aller, H. D., Hughes, P. A., & Latimer, G. E. 1991b, in Variability of Blazars, ed. E. Valtaoja & M. Valtonen (Cambridge: Cambridge Univ. Press), 126
Antonucci, R. R. J., & Ulvestad, J. S. 1985, ApJ, 294, 158
Barbieri, C., Vio, R., Cappellaro, E., & Turatto, M. 1990, ApJ, 359, 63
Bregman, J. N. 1990, ARA&A, 2, 125
Bregman, J. N., et al. 1988, ApJ, 331, 746
Brown, I. W. A. 1987, in Superluminal Radio Sources, ed. J. A. Zensus & T. J. Pearson (Cambridge: Cambridge Univ. Press), 129
Cawthorne, T. V. 1991, in Beams and Jets in Astrophysics, ed. P. A. Hughes (Cambridge: Cambridge Univ. Press), 187
Colla, G., et al. 1970, A&AS, 1, 281
Deeming, T. J. 1975, Ap&SS, 36, 137
Dutta, P., & Horn, P. M. 1981, Rev. Mod. Phys., 53, 497
Edge, D. O., Shakeshaft, J. R., McAdam, W. B., Baldwin, J. E., & Archer, S. 1959, MmRAS, 68, 37
Eilek, J. A., & Hughes, P. A. 1991, in Beams and Jets in Astrophysics, ed. P. A. Hughes (Cambridge: Cambridge Univ. Press), 428
Feigelson, E. D., & Nelson, P. I. 1985, ApJ, 293, 192
Fiedler, R. L., et al. 1987, ApJS, 65, 319
Gabuzda, D. C., & Cawthorne, T. V. 1991, in Variability of Blazars, ed. E. Valtaoja & M. Valtonen (Cambridge: Cambridge Univ. Press), 238
Gabuzda, D. C., Cawthorne, T. V., Roberts, D. H., & Wardle, J. F. C. 1989, ApJ, 347, 701
———. 1992, ApJ, 388, 40
Gregorini, L., Mantovani, F., Eckart, A., Biermann, P., Witzel, A., & Kühr, H. 1984, AJ, 89, 323
Hardee, P. E. 1988, in The Impact of VLBI on Astrophysics and Geophysics, ed. M. J. Reid & J. M. Moran (Dordrecht: Kluwer), 87
Haykin, S., & Kesler, S. 1979, in Nonlinear Methods of Spectral Analysis, ed. S. Haykin (Berlin: Springer), 9
Hughes, P. A., Aller, H. D., & Aller, M. F. 1989a, ApJ, 341, 54
———. 1989b, ApJ, 341, 68
———. 1991, ApJ, 374, 57
Impey, C. 1987, in Superluminal Radio Sources, ed. J. A. Zensus, & T. J. Pearson (Cambridge: Cambridge Univ. Press), 233
Isobe, T., Feigelson, E. D., & Nelson, P. I. 1986, ApJ, 306, 490
Jones, T. W., Rudnick, L., Aller, H. D., Aller, M. F., Hodge, P. E., & Fiedler, R. L. 1985, ApJ, 290, 627
Kraus, J. D., & Andrew, B. H. 1971, AJ, 76, 103
Kühr, H., Witzel, A., Pauliny-Toth, I. I. K., & Nauber, U. 1981, A&AS, 45, 367
Marcaide, J. M., et al. 1990, in Parsec Scale Radio Jets, ed. J. A. Zensus & T. J. Pearson (Cambridge: Cambridge Univ. Press), 59
Marscher, A. P. 1987, in Superluminal Radio Sources, ed. J. A. Zensus & T. J. Pearson (Cambridge: Cambridge Univ. Press), 280
Marscher, A. P., & Gear, W. K. 1985, ApJ, 298, 114
Marscher, A. P., & Shaffer, D. B. 1980, AJ, 85, 668
McHardy, I. 1989, in BL Lac Objects, ed. L. Maraschi, T. Maccacaro, & M.-H. Ulrich (Berlin: Springer), 189
Mutel, R. L. 1990, in Parsec Scale Radio Jets, ed. J. A. Zensus & T. J. Pearson (Cambridge: Cambridge Univ. Press), 98
Mutel, R. L., Phillips, R. B., Su, B., & Bucciferro, R. R. 1990, ApJ, 352, 81
O'Dea, C. P., Barvainis R., & Challis P. M. 1988, AJ, 96, 435
Padrielli, L., et al. 1987, A&AS, 67, 63
Padrielli, L., et al. 1986, A&A, 165, 53
Pauliny-Toth, I. I. K., Wade, C. M., & Heeschen, D. S. 1966, ApJS, 13, 65
Pearson, T. J., & Readhead, A. C. S. 1988, ApJ, 328, 114
Press, W. H. 1978, Comments Ap., 7, 103
Preston. R. A., Morabito, D. D., Williams, J. G., Faulkner, J., Jauncey, D. L., & Nicolson, G. D. 1985, AJ, 90, 1599
Quirrenbach, A., et al. 1991, ApJ, 372, L71
Roberts, D. H., Lehár, J., & Dreher, J. W. 1987, AJ, 93, 968
Romney, J., et al. 1984, A&A, 135, 289
Rudnick, L., & Jones, T. W. 1983, AJ, 88, 518
Rusk, R. E. 1988, Ph.D. thesis, Univ. Toronto
Rusk, R., & Seaquist, E. R. 1985, AJ, 90, 30
Scargle, J. D. 1982, ApJ, 263, 835
Simard-Normandin, M., Kronberg, P. P., & Button, S. 1981, ApJS, 45, 97
Simonetti, J. H., Cordes, J. M., & Heeschen, D. S. 1985, ApJ, 296, 46
Spangler, S., Fanti, R., Gregorini, L., & Padrielli, L. 1989, A&A, 209, 315
Spangler, S., Fey, A., & Mutel, R. 1988, in The Impact of VLBI on Astrophysics and Geophysics, ed. M. J. Reid & J. M. Moran (Dordrecht: Kluwer), 303
Ulrych, T. J., & Ooe, M. 1979, in Nonlinear Methods of Spectral Analysis, ed. S. Haykin (Berlin: Springer), 73
Valtonen, M., et al. 1988, in Active Galactic Nuclei, ed. H. R. Miller & P. J. Wiita (Berlin: Springer), 68
Wardle, J. F. C., & Roberts, D. H. 1988, in The Impact of VLBI on Astrophysics and Geophysics, ed. M. J. Reid & J. M. Moran (Dordrecht: Kluwer), 143
Wehrle, A., Cohen, M. H., Unwin, S. C., Aller, H. D., Aller, M. F., & Nicolson, G. 1991, ApJ, 391, 589
Zhang, Y. F., Marscher, A. P., Shaffer, D. B., Marcaide, J. M., Alberdi, A., & Elósegui, P. 1990, in Parsec Scale Radio Jets, ed. J. A. Zensus & T. J. Pearson (Cambridge: Cambridge Univ. Press), 66